Probing the Scotogenic Dirac Model with FIMP dark matter and $\Delta N_{\rm eff}$*

Shu-Yuan Guo (郭书源)† Man-Yu Zhao (赵曼玉)‡

Department of Physics, Yantai University, Yantai 264005, China

Abstract: We study a feebly interacting massive particle realization of the Scotogenic Dirac Model in which the lightest neutral fermion N_1 serves as a dark matter (DM) candidate produced via the freeze-in or super-WIMP mechanism. The model generates Dirac neutrino masses at one loop, resulting in a rank-2 mass matrix that predicts one almost massless neutrino. We analyze the DM relic density for various next-to-lightest odd particles (NLOPs), finding that coannihilation effects and enhanced annihilation channels are crucial for achieving the correct thermal freeze-out abundance of the NLOP. We provide a detailed analysis of the model's implications for the effective number of relativistic species, $\Delta N_{\rm eff}$, which receives contributions from both a thermal bath of right-handed neutrinos and non-thermal energy injection due to late NLOP decays. Through an extensive parameter scan, we identify the viable parameter space for all NLOP candidates that satisfies constraints from the DM relic density, lepton flavor violation, Big Bang nucleosynthesis, cosmic microwave background, and $\Delta N_{\rm eff}$.

Keywords: neutrino mass, dark matter, neutrino cosmology

DOI: 10.1088/1674-1137/ae1afd **CSTR:** 32044.14.ChinesePhysicsC.50033102

I. INTRODUCTION

The phenomenon of neutrino oscillations [1−6] provides strong evidence that neutrinos must have non-zero masses. Two types of mass are theoretically possible for neutral fermions such as neutrinos: Dirac and Majorana. On the experimental front, extensive efforts have been devoted to searching for lepton number violations—a feature of Majorana neutrinos. In particular, experiments using colliders [7, 8] and neutrinoless-double-beta-decay ($0\nu\beta\beta$) [9−14] searches have yielded no positive signals to date. As a result, the alternative scenario has received increasing attention in recent years [15−54]. To generate the tiny Dirac neutrino masses, an attractive approach is to attribute them to a radiative mechanism that is realized through loop diagrams. The loop suppression naturally explains the smallness of the masses, while the particles running in the loop can carry quantum numbers under a discrete symmetry. This same symmetry can stabilize the lightest particle in the loop, making it a viable dark matter (DM) candidate.

The weakly interacting massive particle (WIMP) paradigm, featuring electroweak-scale particles with weak cross-sections ($\sigma \sim 10^{-26}$ cm^3/s), naturally yields the observed DM density ($\Omega_{\rm DM}h^2 \approx 0.12$) via thermal freeze-out (see [55] for a review). However, this paradigm faces significant challenges arising from null results in direct DM detection [56, 57]. In response, the feebly interacting massive particle (FIMP) scenario has emerged as a compelling alternative [58−62]. Unlike thermal WIMPs, FIMPs are produced via extremely weak couplings, avoiding current experimental bounds while naturally explaining the observed DM abundance.

The Scotogenic Dirac Model, originally proposed in Ref. [20] and later developed with an alternative symmetry realization in Ref. [63], extends the standard model (SM) with right-handed neutrinos ν_R, vector-like fermions N, a scalar doublet Φ, and a scalar singlet χ. Previous work [63] explored the scenario in which the lightest fermion N_1 acts as WIMP DM. This scenario faces significant challenges owing to stringent constraints from lepton flavor violation (LFV) experiments, which severely limit the Yukawa couplings required for efficient thermal relic production. Consequently, achieving the observed relic density requires substantial parameter tuning and relies on annihilation channels mediated by the y_χ coupling. In this work, we propose a novel realization of the Scoto-

Received 25 August 2025; Accepted 3 November 2025; Accepted manuscript online 4 November 2025

* Supported by the NNSFC (12305113), the Natural Science Foundation of Shandong Province (ZR2022QA026) and the Project of Shandong Province Higher Educational Science and Technology Program (2022KJ271)

† E-mail: shyuanguo@ytu.edu.cn

‡ E-mail: manyuzhao@s.ytu.edu.cn

genic Dirac Model in which the lightest neutral fremion N_1 serves as a FIMP DM candidate. This scenario is defined by the extreme suppression of the Yukawa couplings $(y_\Phi)_{\alpha 1}$ and $(y_\chi)_{\alpha 1}$, which ensures that N_1 never enters thermal equilibrium with the SM plasma throughout cosmic history. This FIMP framework not only provides a natural mechanism for DM production but also has a profound impact on neutrino physics, leading to a rank-2 structure for the neutrino mass matrix. This structure predicts one almost massless neutrino state, which is allowed by the oscillation data. We systematically investigate two complementary production mechanisms for N_1. The first is the conventional freeze-in mechanism, in which N_1 is slowly produced via the extremely small Yukawa couplings through decays of heavier Z_2-odd scalars and fermions. The second is the super-WIMP mechanism, in which N_1 is produced by the late decays of a thermally frozen-out next-to-lightest odd particle (NLOP). The identity of the NLOP—whether it is N_2, $\phi_{R,I}$, $\phi^\pm$, or χ—plays a crucial role in shaping the model's phenomenology, directly influencing the DM relic abundance and cosmological observables. A central focus of our analysis is the effective number of relativistic species $\Delta N_{\rm eff}$. We show that $\Delta N_{\rm eff}$ receives contributions from two distinct sources: a thermal component from the primordial bath of right-handed neutrinos and a non-thermal component arising from energy injection owing to late NLOP decays. Our comprehensive parameter scan demonstrates that viable regions of parameter space exist for all possible NLOP candidates, satisfying all current observational constraints from DM relic density, LFV, Big Bang nucleosynthesis (BBN), cosmic microwave background (CMB), and $\Delta N_{\rm eff}$.

The remainder of this paper is organized as follows: Section II introduces the FIMP scotogenic Dirac model and the mechanism for Dirac neutrino mass generation. Section III details the DM relic density calculations. Section IV analyzes the cosmological implications for the effective number of relativistic species. Finally, our conclusions are presented in Section V.

II. MODEL

The Scotogenic Dirac Model was originally proposed in Ref. [20], and a different symmetry realization was presented in [63] by one of the authors. The relevant particles in this model are listed in Table 1. Apart from the SM lepton doublet $F_L = (\nu_L, \ell_L)^T$ and Higgs H, species include the right-handed neutrinos ν_R, three vector-like fermions N, an extra scalar doublet $\Phi \equiv (\phi^+, (\phi_R + i\phi_I)/\sqrt{2})^T$, and a scalar singlet χ. Tree-level Dirac neutrino masses and possible Majorana masses of ν_R and N are forbidden owing to the existence of Z_3.

The introduction of the new particles in Table 1 would result in the following interactions:

Table 1. Particles and symmetries in the Scotogenic Dirac Model.

	F_L	H	ν_R	N	Φ	χ
$SU(2)_L$	2	2	1	1	2	1
$U(1)_Y$	−1/2	1/2	0	0	1/2	0
Z_3	0	0	ω	ω	ω	0
Z_2	+	+	+	-	-	-

$$-\mathcal{L}_{\rm new} \supset \left(y_\Phi \overline{F_L}\tilde{\Phi} N + y_\chi \overline{\nu_R}\chi N + \text{h.c.}\right) + m_N \overline{N} N, \tag{1}$$

where $\tilde{\Phi} \equiv i\sigma_2 \Phi^\star$. The relevant scalar potential terms are expressed as

$$\begin{aligned} V = & -\mu_H^2 H^\dagger H + \mu_\Phi^2 \Phi^\dagger \Phi + \frac{1}{2}\mu_\chi^2 \chi^2 + \frac{1}{2}\lambda_1 (H^\dagger H)^2 \\ & + \frac{1}{2}\lambda_2 (\Phi^\dagger \Phi)^2 + \frac{1}{4!}\lambda_3 \chi^4 \\ & + \lambda_4 (H^\dagger H)(\Phi^\dagger \Phi) + \frac{1}{2}\lambda_5 (H^\dagger H)\chi^2 \\ & + \frac{1}{2}\lambda_6 (\Phi^\dagger \Phi)\chi^2 + \lambda_7 (H^\dagger \Phi)(\Phi^\dagger H) \\ & + \left(\mu \Phi^\dagger H \chi + \text{h.c.}\right). \end{aligned} \tag{2}$$

The scalar singlet χ is set as real for simplicity. The μ-term in Eq. (2) is the source that softly breaks the Z_3 symmetry; hence, it is natural to maintain it at a small value. The one-loop neutrino mass (as illustrated in Fig. 1) is then generated as

$$\begin{aligned} (M_\nu)_{\alpha\beta} = & \frac{\sin 2\theta}{32\pi^2\sqrt{2}} \sum_{k=1,2,3} (y_\Phi)_{\alpha k} (y_\chi^*)_{\beta k} m_{N_k} \\ & \times \left(\frac{m_1^2}{m_1^2 - m_{N_k}^2} \ln \frac{m_1^2}{m_{N_k}^2} - \frac{m_2^2}{m_2^2 - m_{N_k}^2} \ln \frac{m_2^2}{m_{N_k}^2} \right). \end{aligned} \tag{3}$$

The lower indices $\alpha(\beta)$ and k represent different generations of leptons and Ns. The angle θ in Eq. (3) originates from mixing between the real component of the scalar doublet Φ and singlet χ. When the SM Higgs H acquires its vacuum expectation value v after electroweak spontaneous symmetry breaking, the angle is quantitatively fixed as

$$\tan 2\theta = \frac{2\sqrt{2}\mu v}{\mu_\Phi^2 - \mu_\chi^2 + (\lambda_4 - \lambda_5)v^2}. \tag{4}$$

The term $m_{1(2)}^2$ in Eq. (3) indicates eigenvalues of the $\chi - \phi_R$ mixing mass-square matrix

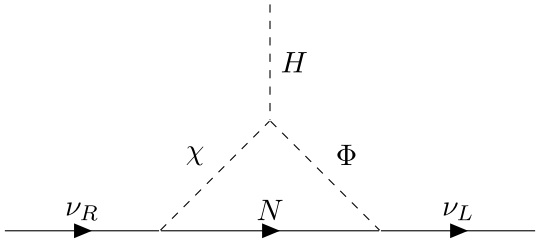

Fig. 1. One-loop neutrino mass in the Scotogenic Dirac Model.

$$m^2_{(\chi,\phi_R)} = \begin{pmatrix} \mu_\chi^2 + \lambda_5 v^2 & \sqrt{2}\mu v \\ \sqrt{2}\mu v & \mu_\Phi^2 + (\lambda_4+\lambda_7)v^2 \end{pmatrix}. \tag{5}$$

Treating μ as a tiny parameter results in small mixing, justifying the approximation $m_{1(2)} \approx m_{\chi(\phi_R)}$. Hence, hereafter, we use m_χ and m_{ϕ_R}. The masses of the other scalars are $m_h^2 = 2\lambda_1 v^2$, $m_{\phi^\pm}^2 = \mu_\Phi^2 + \lambda_4 v^2$, $m_{\phi_I}^2 = \mu_\Phi^2 + (\lambda_4+\lambda_7)v^2$. Here, h is the observed 125 GeV boson.

The assignment of Z_2 in Table 1 would cause particles in the loop of Fig. 1 to be in the dark sector, and the lightest one naturally serves as the DM particle candidate. In Ref. [63], we conducted a detailed study on the situation in which N_1 is a WIMP-type DM particle. In this work, however, we explore an alternative scenario in which the DM candidate N_1 is a FIMP. The FIMP nature of N_1 implies that the Yukawa couplings $(y_\Phi)_{\alpha 1}$ and $(y_\chi)_{\alpha 1}$ are extremely small. This setup significantly distinguishes the model from the conventional WIMP Dirac scotogenic framework. From Eq. (3), we observe that the neutrino mass matrix M_ν is approximately of rank-2, which is a direct consequence of the suppressed couplings $(y_\Phi)_{\alpha 1}$ and $(y_\chi)_{\alpha 1}$. This structure predicts that one of the three neutrino mass eigenstates is almost massless, which remains consistent with the oscillation data requiring at least two massive neutrinos.

The Yukawa interactions y_Φ could mediate the processes leading to LFV, which is extremely suppressed in the SM. Experimentally, the most stringent limits arise from the rare decays $\ell_\alpha \to \ell_\beta \gamma$. The decay branching ratio is calculated as

$$\begin{aligned}\mathrm{Br}(\ell_\alpha \to \ell_\beta \gamma) &= \mathrm{Br}(\ell_\alpha \to \ell_\beta \nu_\alpha \bar{\nu}_\beta) \\ &\times \frac{3\alpha_{\rm em}}{16\pi G_F^2}\left|\sum_i \frac{(y_\Phi)_{\beta i}(y_\Phi^*)_{\alpha i}}{m^2_{\phi^\pm}} j\left(\frac{m^2_{N_i}}{m^2_{\phi^\pm}}\right)\right|^2, \end{aligned} \tag{6}$$

where $j(r) = \left(1-6r+3r^2+2r^3-6r^2\ln r\right)/\left(12(1-r)^4\right)$. The latest result from MEG II reported the limit as $\mathrm{Br}(\mu \to e\gamma) \lesssim 1.5\times 10^{-13}$ [64]. This could be translated into a limit on y_Φ as $(y_\Phi)_{\alpha 2,3} \lesssim 0.01$, if we assume that the new masses are not far away from the electroweak scale. When combined with the neutrino mass in Eq. (3), and noting that the mixing angle θ is small (as it reflects the Z_3-breaking parameter μ in Eq. (4)), we deduce that $(y_\chi)_{\alpha 2,3}$ must be comparable to or larger than $(y_\Phi)_{\alpha 2,3}$. For example, with $\sin 2\theta \sim 10^{-5}$ and $(y_\Phi)_{\alpha 2,3} \lesssim 0.01$, reproducing the observed neutrino masses requires $(y_\chi)_{\alpha 2,3} \gtrsim 0.01$.

III. DM RELIC DENSITY

The residual Z_2 symmetry confines loop particles to the dark sector, with the lightest Z_2-odd particle serving as the DM candidate. In [63], we analyzed the scenario in which the fermion N_1 acts as WIMP DM. We found that DM annihilation via y_Φ is difficult to achieve at the correct relic density. This limitation arises because the Yukawa coupling y_Φ faces stringent constraints from LFV. The y_Φ that is compatible with these LFV constraints substantially suppresses N_1 annihilation cross-sections, resulting in DM overproduction that is excluded by cosmological observations. Consequently, the dominant annihilation must proceed through y_χ.

However, in this work, we attempt a FIMP realization of DM N_1. The feeble interaction strength would retain N_1 always out of equilibrium. Thus, the key means of producing N_1 are decays of heavier Z_2-odd particles. The dominant contributions are from decays of scalars:

$$\Gamma_{\phi_{R,I}\to N_1\bar{\nu}_\alpha} = \frac{|(y_\Phi)_{\alpha 1}|^2}{32\pi}\frac{(m^2_{\phi_{R,I}} - m^2_{N_1})^2}{m^3_{\phi_{R,I}}}, \tag{7}$$

$$\Gamma_{\phi^+\to N_1\ell^+_\alpha} = \frac{|(y_\Phi)_{\alpha 1}|^2}{16\pi}\frac{(m^2_{\phi^+} - m^2_{N_1})^2}{m^3_{\phi^+}}, \tag{8}$$

$$\Gamma_{\chi\to N_1\bar{\nu}_\alpha} = \frac{|(y_\chi)_{\alpha 1}|^2}{16\pi}\frac{(m^2_{\chi} - m^2_{N_1})^2}{m^3_{\chi}}. \tag{9}$$

Additional production channels involve decays from $N_{2,3}$:

$$\Gamma_{N_{2,3}\to N_1\ell^-_\alpha\ell^+_\beta} = \frac{|(y_\Phi)_{\beta 1}|^2\,|(y_\Phi)_{\alpha 2,3}|^2}{6144\pi^3}\frac{m^3_{N_{2,3}}(m^2_{N_{2,3}} - 2m^2_{N_1})}{m^4_{\phi^+}}, \tag{10}$$

$$\begin{aligned}\Gamma_{N_{2,3}\to N_1\nu_\alpha\bar{\nu}_\beta} &= \frac{m^3_{N_{2,3}}(m^2_{N_{2,3}} - 2m^2_{N_1})}{6144\pi^3} \\ &\times\left(\sum_{\phi_R,\phi_I}\frac{|(y_\Phi)_{\beta 1}|^2\,|(y_\Phi)_{\alpha 2,3}|^2}{m^4_\phi} + \frac{|(y_\chi)_{\beta 1}|^2\,|(y_\chi)_{\alpha 2,3}|^2}{m^4_\chi}\right).\end{aligned} \tag{11}$$

Fermionic decay contributions remain subdominant owing to both three-body phase space suppression and additional Yukawa coupling factors. Moreover, decays into $\bar{N}_1$ and decays of $\bar{N}_2 \to N_1(\bar{N}_1)$, whose widths are similar to those in Eqs. (7) to (11), should also be considered to obtain the total abundance of DM. To ensure N_1 remains

out of thermal equilibrium, the decay rate should be smaller than the Hubble expansion rate. A rough estimate requires the Yukawa coupling $(y_{\Phi,\chi})_{\alpha 1} \lesssim 10^{-7}$ for scalar masses at O(TeV).

The evolution of DM and the relevant particles is governed by the following Boltzmann equations:

$$\frac{\mathrm{d}Y_{N_1+\bar{N}_1}}{\mathrm{d}z} = k^* z \sum_X \left(\tilde{\Gamma}_{X\to N_1} + \tilde{\Gamma}_{X\to \bar{N}_1}\right) Y_X, \tag{12}$$

$$\begin{aligned}\frac{\mathrm{d}Y_X}{\mathrm{d}z} =& k^* z \sum_A \tilde{\Gamma}_{A\to X}\left(Y_A - \frac{Y_A^{\rm eq}}{Y_X^{\rm eq}} Y_X\right) \\ & - k^* z \sum_B \tilde{\Gamma}_{X\to B}\left(Y_X - \frac{Y_X^{\rm eq}}{Y_B^{\rm eq}} Y_B\right) \\ & + \frac{k}{z^2}\langle\sigma v\rangle_{\rm SM\to X\bar{X}}\left((Y_{\rm SM}^{\rm eq})^2 - \frac{(Y_{\rm SM}^{\rm eq})^2}{(Y_X^{\rm eq})^2} Y_X Y_{\bar{X}}\right).\end{aligned} \tag{13}$$

Here, $X = \phi_R, \phi_I, \phi^\pm, \chi, N_{2,3}(\bar{N}_{2,3})$ represents all Z_2-odd particles that could decay into DM. The evolution of a specific X is affected by three types of processes: decays of heavier A into X, decays of X into lighter B, and SM pairs annihilating into X pairs. The dimensionless parameter z is defined as the ratio of the DM mass to the evolution temperature, *i.e.*, $z \equiv m_{N_1}/T$. The parameter k^* is expressed as $k^* = \sqrt{45/(4\pi^3 g^*)} M_{\rm Pl}/m_{N_1}^2$, where g^* is the effective number of degrees of freedom of the relativistic particles and $M_{\rm Pl} = 1.2\times 10^{19}$ GeV is the Planck mass. The thermal decay width $\tilde{\Gamma}_{i\to j}$ is defined as $\tilde{\Gamma}_{i\to j} = \Gamma_{i\to j} K_1/K_2$, where K_1 and K_2 denote the first and second order of modified Bessel functions of the second kind, respectively. $Y_i^{\rm eq}$ represents the abundance in equilibrium for species i.

In practice, we write the model using `FeynRules` [65] and the output model files are used to calculate the relic density with `micrOmegas` [66]. We present the results of this calculation in Fig. 2, which illustrates the comoving yield of N_1 as a function of the cosmological variable $z = m_{N_1}/T$ for several benchmark values of the feeble Yukawa couplings $(y_\Phi)_{\alpha 1}$ and $(y_\chi)_{\alpha 1}$. For simplicity in this analysis, we set these couplings to be equal, *i.e.*, $(y_\Phi)_{\alpha 1} = (y_\chi)_{\alpha 1}$, while the remaining model parameters are fixed to the values specified in Table 2. The resulting evolution curves exhibit the characteristic hallmark of the freeze-in mechanism. At high temperatures ($z \ll 1$), the abundance of N_1 is negligible. As the universe cools, N_1 is slowly but steadily produced from decays of the heavier Z_2-odd particles. The yield increases progressively until the source particles become thermally suppressed and depleted, at which point the comoving number density of N_1 "freezes in" and remains constant. For reference, the observed DM relic density, $\Omega_{\rm DM}h^2 \approx 0.12$, is indicated by a horizontal dashed line. We demonstrate that a viable parameter point corresponding to the specific coupling strength $(y_\Phi)_{\alpha 1} = (y_\chi)_{\alpha 1} = 5\times 10^{-12}$ successfully saturates the observed DM density.

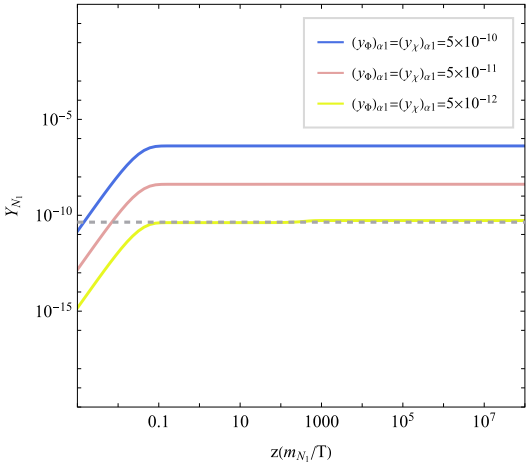

Fig. 2. (color online) Evolution of DM through freeze-in. The parameters used are listed in Table 2.

In addition to the conventional freeze-in mechanism, DM can also be produced via the late decay of a thermally frozen-out NLOP, a scenario known as the "super-WIMP" mechanism [67]. In this framework, heavier Z_2-odd particles decay predominantly into the NLOP in the early universe, as these transitions are not suppressed by small couplings. The NLOP is initially in thermal equilibrium with both the SM and other Z_2-odd particles, but as the universe cools, its interaction rate dereases below the Hubble expansion rate, leading to decoupling and the freeze-out of its comoving number density. Subsequently, the NLOP undergoes a highly suppressed decay into stable DM owing to extremely weak coupling.

Table 2. Parameter sets used in Figs. 2 and 3. Masses are expressed in GeV.

m_{N_1}	m_{N_2}	m_{N_3}	m_{ϕ_R}	$m_{\phi_I,\phi^\pm}$	m_χ	$(y_{\Phi,\chi})_{\alpha 1}$	$(y_\Phi)_{\alpha 2,3}$	$(y_\chi)_{\alpha 2,3}$	λ_5	Figure
10	800	800	800	800	800	$5\times10^{-10,-11,-12}$	10^{-3}	10^{-2}	10^{-3}	Fig. 2
10	600/770	800	800	800	800	5×10^{-13}	10^{-2}	10^{-2}	10^{-3}	Fig. 3(a)
10	300	800	800	800	800	5×10^{-13}	10^{-2}	0.1/0.3	10^{-3}	Fig. 3(b)
500	800	800	750	800	800	5×10^{-13}	10^{-3}	10^{-2}	10^{-3}	Fig. 3(c)
10	800	800	800	800	550	5×10^{-13}	10^{-3}	$0.5/10^{-3}$	10^{-3}/0.02	Fig. 3(d)

This results in a long-lived NLOP and a delayed, non-thermal production of DM that persists until the NLOP population fully decays. The resulting DM relic abundance is totally fixed from the NLOP's freeze-out density:

$$\Omega_{N_1}^{\text{super-WIMP}} = \frac{m_{N_1}}{m_{\text{NLOP}}}\Omega_{\text{NLOP}}^{\text{freeze-out}}. \tag{14}$$

This production mechanism is illustrated in Fig. 3, which shows several distinct realizations of the NLOP within our model.

Figs. 3(a) and 3(b) depict scenarios in which the NLOP is the fermionic state N_2. Its freeze-out is driven by annihilations into SM leptons, mediated by the Yukawa couplings $(y_\Phi)_{\alpha 2}$ or $(y_\chi)_{\alpha 2}$. However, as shown in [62], LFV constraints severely limit $(y_\Phi)_{\alpha 2}$, suppressing the annihilation cross-section and leading to an overproduction of N_2 if this coupling dominates. Additional mechanisms are required to achieve the correct relic abundance. One such mechanism is coannihilation: when N_2 is almost degenerate in mass with other Z_2-odd states, their combined interactions enhance the effective annihilation rate. Fig. 3(a) compares two benchmarks, m_{N_2} = 600 GeV and 770 GeV, with the other odd particles fixed at 800 GeV. The heavier N_2 case benefits from stronger coannihilation effects, yielding a reduced freeze-out abundance that is consistent with observations. Alternatively, in our model, the coupling $(y_\chi)_{\alpha 2}$ opens an additional t-channel annihilation via exchange of the scalar singlet χ, producing neutrino final states. As demonstrated in Fig. 3(b), increasing $(y_\chi)_{\alpha 2}$ significantly enhances the annihilation rate, thereby reducing $\Omega_{N_2}^{\text{freeze-out}}$ and bringing the final DM density into agreement with the cosmological data.

In scenarios in which the scalar doublet Φ serves as the NLOP, we focus on its neutral real component ϕ_R as the representative case (with ϕ_I and $\phi^\pm$ exhibiting similar dynamics). ϕ_R annihilates efficiently through electroweak gauge interactions (e.g., $\phi_R\phi_R \to W^+W^-, ZZ$), resulting in strong thermal coupling. The correct relic

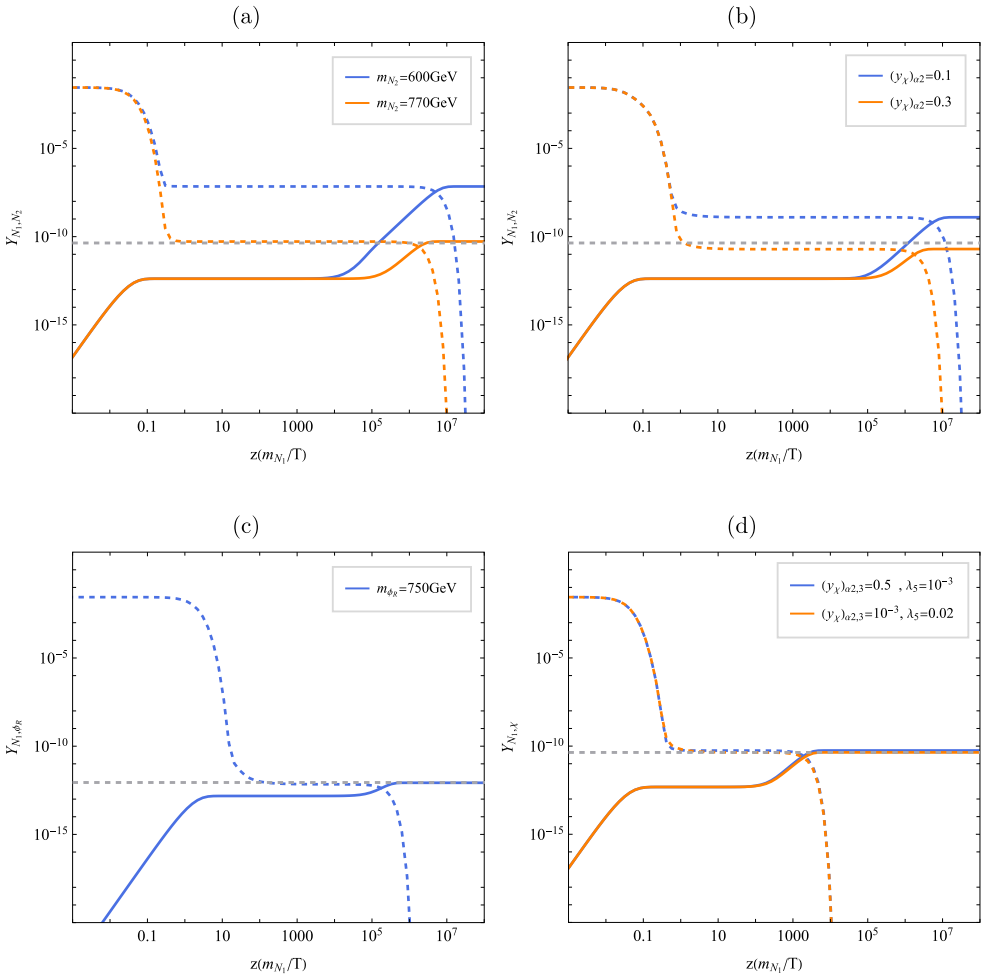

Fig. 3. (color online) Evolution of DM and NLOP under the "super-WIMP" mechanism. N_2 is selected as the NLOP in the upper two subfigures, while ϕ_R and χ are selected as the NLOP in the lower two subfigures, respectively. The parameters used are listed in Table 2.

abundance is only achieved in the mass region of $m_{\phi_R} > 500\,\text{GeV}$ (or $m_{\phi_R} < m_W$) [68–71]. In Fig. 3(c), we consider a benchmark mass $m_{\phi_R} = 750\,\text{GeV}$. A moderate mass hierarchy between N_1 and ϕ_R is required (hence, we set $m_{N_1} = 500\,\text{GeV}$), as the freeze-out abundance of ϕ_R is typically not significantly larger than the observed DM density [62].

For completeness, we also consider the phenomenology of the charged component $\phi^\pm$ when it acts as the NLOP. Being electrically charged and long-lived (owing to suppressed decays into N_1), $\phi^\pm$ behaves as a long-lived charged particle. The ATLAS Collaboration has recently searched for such states in 140 fb^{-1} of pp collision data at $\sqrt{s} = 13\,\text{TeV}$ using signatures based on high specific ionization energy loss and time-of-flight measurements [72]. Interpreting their results in the context of stau-to-gravitino decays, ATLAS excludes masses up to 560 GeV for such long-lived charged particles. Furthermore, in Fig. 4, we present the assessment of the projected sensitivity of future long-lived particle detector MATHUSLA [73]. Fig. 4 shows the projected reach in the mass-decay length plane of a long-lived $\phi^\pm$ [73], which is assumed to be pair-produced via Drell-Yan processes at the 14 TeV HL-LHC and to decay into DM. The reconstruction efficiency is assumed to be 0.5–1. The contours indicate regions where at least four events are expected with 3 ab^{-1}. In Fig. 4, we also show the Yukawa coupling strength as a function of the mass and decay length. Nevertheless, for the parameter space that yields the correct DM relic density, MATHUSLA's projected coverage remains limited to only a marginal segment.

Finally, we consider the scenario in which the scalar singlet χ serves as the NLOP. The annihilation of χ in the early universe is governed by three key parameters: the Yukawa coupling y_χ, Higgs portal coupling λ_5, and trilinear scalar coupling μ. Annihilation through y_χ proceeds via t-channel exchange of the heavy neutral fermions $N_{2,3}$, yielding neutrino final states. Alternatively, χ can annihilate into SM particle pairs—such as $b\bar{b}$, WW, or ZZ—through s-channel Higgs exchange, mediated by the $\lambda_5(H^\dagger H)\chi^2$ interaction. Motivated by the requirement of naturally small neutrino masses and the preservation of an approximate global symmetry in the scalar sector, we consider the coupling μ as hierarchically suppressed throughout this analysis. This naturalness argument renders μ negligible for thermal processes, leaving y_χ and λ_5 as the dominant drivers of χ's annihilation dynamics. To illustrate the viable parameter space, we examine two representative benchmark scenarios. The first features a large Yukawa coupling $(y_\chi)_{2,3} = 0.5$ with a small Higgs portal $\lambda_5 = 10^{-3}$, favoring annihilation into neutrinos. The second adopts a larger portal coupling $\lambda_5 = 0.02$ while maintaining $(y_\chi)_{2,3} = 10^{-3}$ small, enhancing annihilation into SM states via Higgs mediation. As shown in Fig. 3(d), both configurations yield a χ freeze-out abundance that, following subsequent decay into N_1, reproduces the observed DM relic density. This demonstrates the flexibility of the singlet χ NLOP scenario in achieving the correct DM yield through distinct but equally viable annihilation pathways.

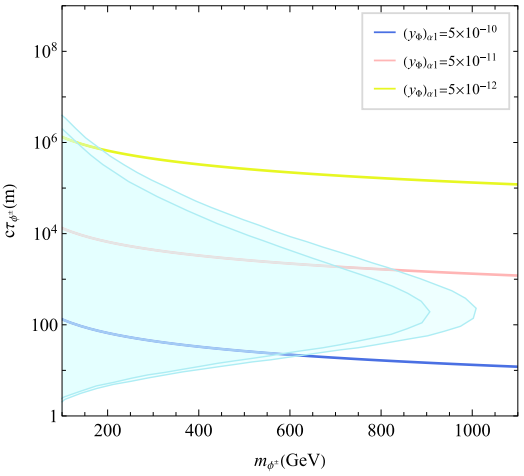

Fig. 4. (color online) Projected detection capabilities of MATHUSLA for a long-lived $\phi^\pm$ in the mass-decay length plane. The band shows that the efficiencies vary from 0.5 to 1. The colored lines correspond to different strengths of Yukawa coupling between $\phi^\pm$ and the DM.

IV. CONSTRAINTS FROM N_{eff}

The Dirac nature of neutrinos necessitates both left-handed (ν_L) and right-handed (ν_R) chiral components. The existence of ν_R contributes additional relativistic degrees of freedom, thereby increasing the radiation energy density in the early universe. This contribution is commonly parameterized by the effective number of relativistic species, which is defined as

$$N_{\text{eff}} = \frac{8}{7}\left(\frac{11}{4}\right)^{4/3}\frac{\rho_{\nu_L}+\rho_{\nu_R}}{\rho_\gamma} = 3\left(\frac{11}{4}\right)^{4/3}\left[\left(\frac{T_{\nu_L}}{T_\gamma}\right)^4+\left(\frac{T_{\nu_R}}{T_\gamma}\right)^4\right]. \quad (15)$$

Within the SM, the effective number of relativistic species is precisely calculated as $N_{\text{eff}}^{\text{SM}} = 3.045$ [74–76], incorporating effects from neutrino oscillations, non-thermal spectral distortions, and finite-temperature corrections. Any deviation from this value owing to physics beyond the SM is typically expressed as $\Delta N_{\text{eff}} \equiv N_{\text{eff}} - N_{\text{eff}}^{\text{SM}}$. The Planck2018 results provide the most accurate and stringent constraint to date, yielding $\Delta N_{\text{eff}} \leq 0.285$ at the 2σ confidence level [77]. The upcoming CMB-S4 experiment is projected to improve the sensitivity significantly, with a forecasted reach of $\Delta N_{\text{eff}} \leq 0.06$ at the same confid-

ence level [78].

A. Thermal contribution

In the early hot universe, all particles except for the FIMP N_1 were in thermal equilibrium with the SM plasma. As the universe expanded and cooled, the dark plasma—comprising the scalar singlet χ, fermion singlets $N_{2,3}$, and right-handed neutrinos ν_R—gradually decoupled from the SM plasma. However, partial thermal equilibrium was maintained within the dark plasma owing to the large Yukawa coupling y_χ. Interactions between the dark plasma and SM plasma can occur through either $N_{2,3}$ or χ. For $N_{2,3}$, interactions with the SM are mediated by the coupling y_Φ, with the scattering amplitude scaling as $|y_\Phi|^2$. In contrast, χ couples with the SM either via t-channel Higgs exchange or through a contact interaction with Higgs, with the scattering amplitude proportional to λ_5. Owing to stringent constraints from LFV, y_Φ is typically too small to support significant interactions. As a result, the dominant portal between the dark plasma and SM is mediated by χ. When χ eventually decouples from the SM plasma, the temperature of the right-handed neutrinos ν_R starts to deviate from that of the SM thermal bath. The decoupling temperature $T_{\rm dec}$ is determined by the condition $\Gamma_{\rm el}(T_{\rm dec}) = H(T_{\rm dec})$, where $\Gamma_{\rm el} \equiv \sum n_{\rm SM}\langle\sigma v\rangle_{\chi\,{\rm SM}\to\chi\,{\rm SM}}/(m_\chi/T)$ denotes the effective elastic scattering rate between χ and SM particles, accounting for the number of scatterings required to transfer energy of the order T. In Fig. 5, we show the ratio $\Gamma_{\rm el}/H$ as a function of the temperature for different values of λ_5. The dashed line, corresponding to $\Gamma_{\rm el}/H = 1$, indicates the condition for decoupling. The temperature ratio $T_{\nu_R}/T_{\rm SM}$ can be determined using entropy conservation:

$$\frac{T_{\nu_R}}{T_{\rm SM}} = \left(\frac{g^{*s}_{\rm DP}}{g^{*s}_{\rm SM}}\bigg|_{T_{\rm dec}}\frac{g^{*s}_{\rm SM}}{g^{*s}_{\rm DP}}\right)^{1/3}, \tag{16}$$

where g^{*s}_X denotes the effective number of relativistic degrees of freedom with respect to the entropy density in the X plasma ("DP" refers to dark plasma). The evaluation at $T_{\rm dec}$ indicates that the ratio is set at the dark plasma decoupling temperature. The evolution of $T_{\nu_R}/T_{\rm SM}$ is shown in Fig. 5 for different choices of the dark plasma decoupling temperature. The later the dark plasma decouples (which corresponds to a larger λ_5, and ν_R being heated more efficiently by the SM plasma over a longer period), the higher temperature ratio that is reached. This finally results in a larger contribution to the effective number of relativistic species.

B. Non-thermal contribution from delayed decay of NLOP

In addition to thermal contributions from ν_R, the delayed decay of the NLOP —particularly during the BBN or CMB epochs—can leave observable imprints on cosmological data. Several studies have examined the late decays of heavy relics into electron-positron pairs [79] or neutrinos [80], and constraints have been derived based on their effects on BBN, CMB anisotropies, and spectral distortions. In our model, the NLOP candidates include N_2, $\phi_{R,I}$, $\phi^\pm$, and χ. (The roles of ϕ_R and ϕ_I as the NLOP are entirely analogous, and therefore, the following discussion on ϕ_R as the NLOP applies equally to ϕ_I.) Among these, N_2 and $\phi^\pm$ can decay into SM charged leptons. Exotic electromagnetic (EM) energy injection is tightly constrained by cosmology. CMB observations (*e.g.*, Planck) limit such injection as it alters recombination and distorts the temperature and polarization spectra, while COBE-FIRAS rules out spectral distortions from

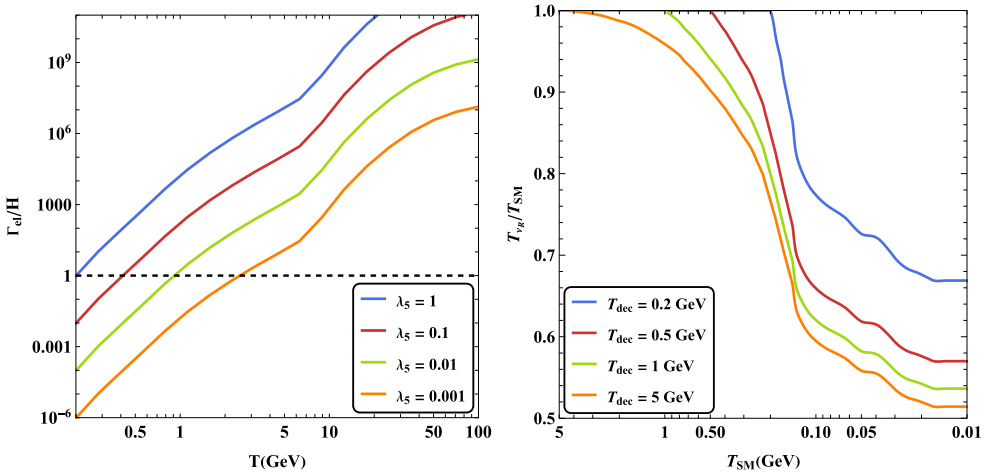

Fig. 5. (color online) (Left panel) Ratio of $\Gamma_{\rm el}/H$ as a function of temperature for different choices of λ_5. Here, we have selected $m_\chi = 100$ GeV for demonstration. (Right panel) Evollution of ratio T_{ν_R}/T_γ for different dark plasma decoupling temperatures.

early injection. During BBN, excess energy disrupts light-element abundances, conflicting with the observed D and ^{4}He. Long-lived N_2 and $\phi^\pm$ with lifetimes between 3×10^4 s and recombination are strongly disfavored unless almost degenerate with the DM (hence minimizing energy release) [79, 81–83]. In this work, we impose a conservative upper bound, requiring the lifetimes of N_2 and $\phi^\pm$ to be less than 3×10^4 s. For scenarios in which ϕ_R or χ is the NLOP, their delayed decays can inject energy into the left- or right-handed neutrinos, thereby altering the neutrino temperatures. The evolution of T_{ν_L}, T_{ν_R}, and T_γ is governed by the following system of differential equations:

$$\begin{aligned}
\frac{\mathrm{d}T_{\nu_L}}{\mathrm{d}t} &= -HT_{\nu_L} + \frac{\dfrac{\delta\rho_{\nu_L}}{\delta t} + \varepsilon^{\nu_L}_{\rm NLOP}\dfrac{\rho_{\rm NLOP}}{\tau_{\rm NLOP}}}{3\dfrac{\partial\rho_{\nu_L}}{\partial T_{\nu_L}}},\\
\frac{\mathrm{d}T_{\nu_R}}{\mathrm{d}t} &= -HT_{\nu_R} + \frac{\varepsilon^{\nu_R}_{\rm NLOP}\dfrac{\rho_{\rm NLOP}}{\tau_{\rm NLOP}}}{3\dfrac{\partial\rho_{\nu_R}}{\partial T_{\nu_R}}},\\
\frac{\mathrm{d}T_\gamma}{\mathrm{d}t} &= -\frac{4H\rho_\gamma + 3H(\rho_e+p_e) + \dfrac{\delta\rho_{\nu_L}}{\delta t}}{\dfrac{\partial\rho_\gamma}{\partial T_\gamma} + \dfrac{\partial\rho_e}{\partial T_\gamma}}.
\end{aligned} \tag{17}$$

Here, ρ and p denote the energy and pressure densities, respectively. $\rho_{\rm NLOP}$ represents the energy density of the NLOP, which evolves as

$$\frac{\mathrm{d}\rho_{\rm NLOP}}{\mathrm{d}t} = -3H\rho_{\rm NLOP} - \frac{\rho_{\rm NLOP}}{\tau_{\rm NLOP}}. \tag{18}$$

$\delta\rho/\delta t$ in Eq. (17) represents the energy transfer rate between the SM neutrinos and EM plasma due to weak interactions, as detailed in Refs. [84, 85]. The parameter $\varepsilon^{\nu_L(\nu_R)}_{\rm NLOP} = (m^2_{\rm NLOP} - m^2_{N_1})/(2m^2_{\rm NLOP})$ quantifies the fraction of the decaying NLOP's rest energy that is effectively deposited into $\nu_L(\nu_R)$[1]. The initial conditions for this system are set at a time when ν_L and the photon bath were in thermal equilibrium ($T_{\nu_L} = T_\gamma$), and the NLOP has not yet decayed. In practice, we begin the numerical calculation at $T_\gamma = 10$ MeV, where ν_L is still coupled to the EM plasma, and any decays occurring earlier would contribute negligibly to the entropy of ν_L or ν_R. The starting temperature of ν_R is fixed by Eq. (16) with setting $T_{\rm SM} = 10$ MeV. Following Ref. [80], we define a dimensionless parameter $f_{\rm NLOP} \equiv \Omega_{\rm NLOP}/\Omega_{\rm DM}$, where $\Omega_{\rm NLOP}$ represents the hypothetical present-day relic abundance of the NLOP if it were stable. Consequently, the initial energy density of the NLOP in Eq. (18) can be expressed as a function of $f_{\rm NLOP}$. In principle, a similar differential equation system should be solved for N_2 or $\phi^\pm$ as the NLOP. However, we have verified that the BBN and CMB constraints (*i.e.* $\tau < 3\times10^4$ s) ensure that any late-decay effects on $\Delta N_{\rm eff}$ are negligible.

We show the evolution of T_{ν_L}/T_γ (solid lines) and T_{ν_R}/T_γ (dashed lines) in Fig. 6, where the first row corresponds to ϕ_R as the NLOP and the second row to χ as the NLOP. The input parameters for Eqs. (17) and (18) are the NLOP energy fraction $f_{\rm NLOP}$, its lifetime $\tau_{\rm NLOP}$, and the temperature of the right-handed neutrino bath at $T_\gamma = 10$ MeV, which is denoted $T_{\nu_R,10}$. We illustrate how different choices of these parameters influence the resulting temperature ratios. In the first colum, $f_{\rm NLOP} = 100$ and $T_{\nu_R,10} = 5$ MeV. The NLOP lifetimes are set to 10^5 s, 10^6 s, and 10^7 s for illustration. As the lifetime of $\phi_R(\chi)$ increases, the delayed decay injects energy into $\nu_L(\nu_R)$ at a later cosmic time, leading to a more pronounced heating effect on $\nu_L(\nu_R)$. In the second column, $\tau_{\rm NLOP} = 10^7$ s and $T_{\nu_R,10} = 5$ MeV, with $f_{\rm NLOP} = 10$, 100, and 1000. A larger $f_{\phi_R}(\chi)$ implies a higher relic density following freeze-out, resulting in greater energy injection into $\nu_L(\nu_R)$ once the decays are complete. In the third column, we examine the impact of varying $T_{\nu_R,10}$ on the temperature ratio evolution. When ϕ_R is the NLOP, its late decay does not affect the thermal history of ν_R, and hence, there is no heating of ν_R. When χ is the NLOP, variations in $T_{\nu_R,10}$ do not influence T_{ν_L}/T_γ because χ decays exclusively into ν_R. A higher $T_{\nu_R,10}$ results in a larger T_{ν_R}/T_γ at the completion of χ decay.

With the time-dependent temperatures T_{ν_L}, T_{ν_R}, and T_γ determined, $\Delta N_{\rm eff}$ can be computed using Eq. (15). It follows from Eq. (17) that the energy injection from NLOP decay into ν_L or ν_R proceeds identically in both scenarios. As a result, the evolution of $\Delta N_{\rm eff}$ is the same whether the NLOP is ϕ_R or χ. We present the resulting $\Delta N_{\rm eff}$ in Fig. 7, where the three subfigures show the effects of varying $\tau_{\rm NLOP}$, $f_{\rm NLOP}$, and $T_{\nu_R,10}$, respectively. The two dashed lines indicate the current experimental limits from Planck [77] and future detection capability from CMB-S4 [78]. A longer NLOP lifetime or a larger $f_{\rm NLOP}$ leads to a more pronounced heating effect, resulting in a higher $\Delta N_{\rm eff}$. A hotter ν_R bath, originating from stronger and more prolonged interactions between the dark plasma and SM plasma, also yields a larger $\Delta N_{\rm eff}$. For completeness, we also show the evolution of $\Delta N_{\rm eff}$ in the scenario in which the contribution from the late decay of the NLOP is negligible, as depicted in the final subfigure of Fig. 7. This occurs when either the NLOP abundance is

1) A portion of the energy injected into ν_L is subsequently transferred to photons and $e^\pm$ via weak interactions, contributing to the thermalization of the EM plasma. The corresponding energy transfer fraction, denoted as $\xi_{\rm EM}$ in Ref. [80], can be read from Fig. 1 of that work. For NLOP masses around the electroweak scale, $\xi_{\rm EM}$ is highly suppressed and effectively negligible. Therefore, we neglect this energy transfer in our analysis.

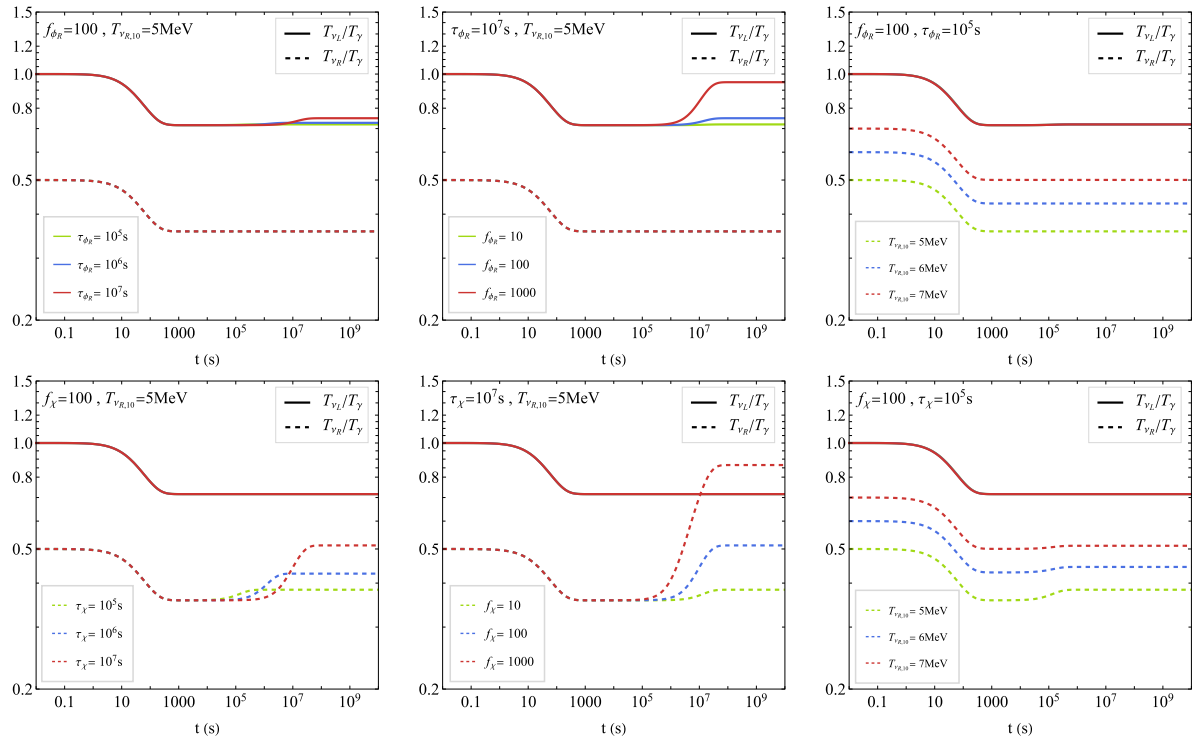

Fig. 6. (color online) Evolution of the temperature ratios T_{ν_L}/T_γ (solid lines) and T_{ν_R}/T_γ (dashed lines). The upper and lower panels show the cases in which ϕ_R and χ are the NLOP, respectively.

small or the NLOP lifetime is sufficiently short. In this limit, $\Delta N_{\rm eff}$ is dominated solely by the thermal contribution from the decoupled ν_R bath. As expected, a higher $T_{\nu_R,10}$ results in a larger $\Delta N_{\rm eff}$ because the ν_Rs contribute more to the radiation density.

C. Combined results

Finally, we perform a comprehensive scan over the full parameter space, imposing constraints from the DM relic density, neutrino mass, LFV, and cosmological observations such as BBN, CMB, and $\Delta N_{\rm eff}$. The scanning ranges for the model parameters are as follows:

$$\begin{aligned} &m_{N_1} \in [1,1000]\,\text{GeV}, \quad m_{\rm NLOP} \in [m_{N_1},1000]\,\text{GeV},\\ &m_{\rm others} \in [m_{\rm NLOP},2000]\,\text{GeV}, \quad (y_{\Phi,\chi})_{\alpha 1} \in [10^{-15},10^{-7}],\\ &(y_\Phi)_{\alpha 2,3} \in [10^{-5},10^{-2}], \quad (y_\chi)_{\alpha 2,3} \in [10^{-3},1],\\ &\lambda_5 \in [10^{-3},1], \quad \sin 2\theta \in [10^{-10},10^{-5}]. \end{aligned} \tag{19}$$

Here, $m_{\rm NLOP}$ is the mass of the NLOP and $m_{\rm others}$ refers to the masses of heavier odd-sector states. The lower bound on $m_{\phi^\pm}$ is set to 560 GeV based on collider searches for long-lived charged particles [72]. The DM relic density is required to lie within the 3σ range of the Planck2018 measurement [77], *i.e.*, $\Omega_{N_1}h^2 \in [0.117,0.123]$. The odd-state masses are scanned up to the energy scale within the reach of current and near-future experiments. The couplings $(y_{\Phi,\chi})_{\alpha 1}$ are bounded from above to ensure that DM remains out of thermal equilibrium. The couplings $(y_\Phi)_{\alpha 2,3}$ are constrained by LFV bounds to be less than 10^{-2}, while $(y_\chi)_{\alpha 2,3}$ are selected to reproduce observed neutrino masses. The mixing parameter $\sin 2\theta$ is restricted to below 10^{-5} on naturalness grounds—because $\theta = 0$ (or equivalently $\mu = 0$) enhances the model symmetry. The quartic coupling λ_5 is scanned down to 10^{-3}, as the thermal contribution to $\Delta N_{\rm eff}$ is no longer significant for smaller values.

As discussed in the previous subsection, we impose a conservative upper limit of $\tau < 3\times 10^4$ s on the lifetime of the NLOP when it is either the charged scalar $\phi^\pm$ or neutral fermion N_2. This bound arises because EM energy injection from late decays can alter light element abundances during BBN and distort CMB anisotropies. However, when the NLOP is the neutral scalar ϕ_R, the constraints are significantly relaxed, as its dominant decays inject energy primarily into neutrinos, rather than the EM plasma. In this case, we adopt the bounds from Ref. [80], which depend on the effective energy transfer parameter $f_{\phi_R}\varepsilon_{\phi_R}$ and are displayed as the blue curve in Fig. 8. In the scan, parameter points satisfying the DM relic density condition are colored pink. Among these, points that additionally satisfy constraints from the neutrino mass and LFV processes are highlighted in green. Points that further pass the BBN and CMB bounds are shown in red. One can observe that the BBN and CMB limits ex-

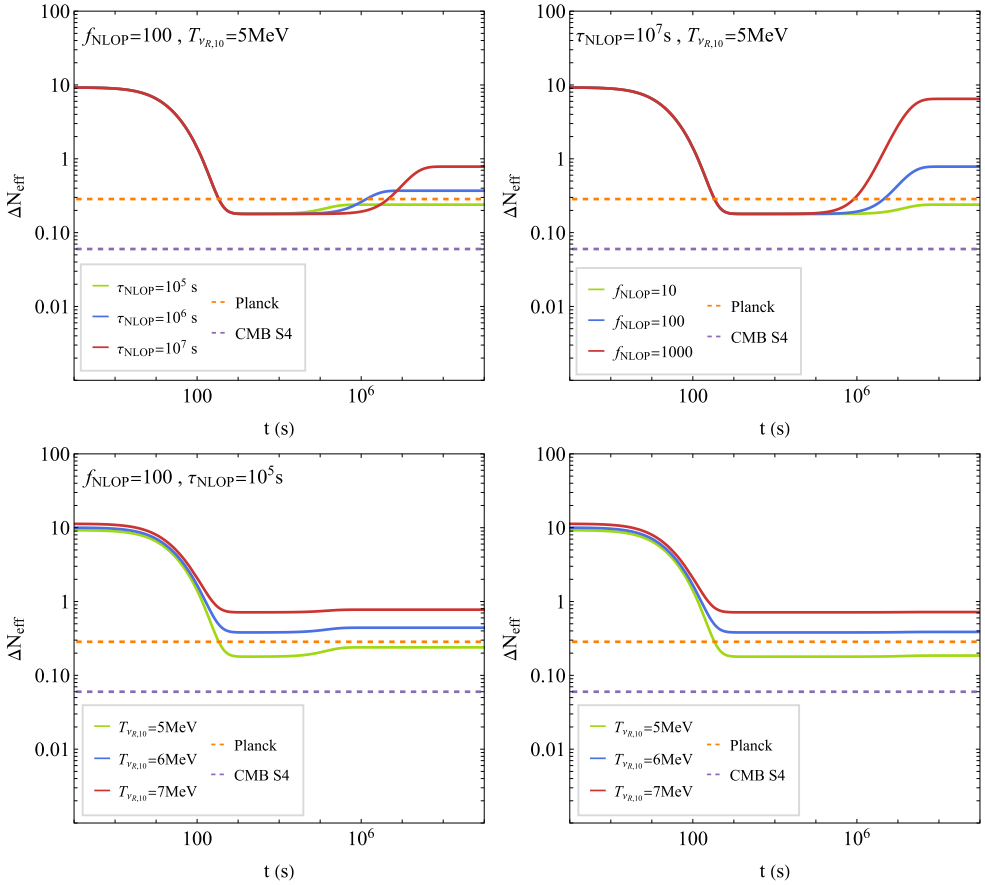

Fig. 7. (color online) Evolution of $\Delta N_{\rm eff}$ for varying $\tau_{\rm NLOP}$, $f_{\rm NLOP}$, and $T_{\nu_R,10}$. The final subfigure illustrates the scenario in which $\Delta N_{\rm eff}$ is dominated by thermal contributions.

clude long-lived ϕ_R with lifetimes $\gtrsim 10^4$–10^7 s, although the constraints are significantly weakened when the energy transferred to the neutrino sector is small. When the NLOP is the scalar χ, which decays directly into the right-handed neutrino, there are no direct BBN or CMB constraints, as the decay products are sterile and do not interact with the thermal bath.

In Fig. 9, we present the scanning results in the $m_{\rm NLOP}$–m_{N_1} plane, considering different particles as the NLOP. Constraints from the DM relic density, neutrino mass and LFV, BBN and CMB, and $\Delta N_{\rm eff}$ are applied successively. The color coding follows the same progression as that in Fig. 8. Finally, points that also satisfy the $\Delta N_{\rm eff}$ constraint are marked in blue, indicating full consistency with all observational requirements. The DM relic density receives contributions from both the freeze-in and super-WIMP mechanisms, as discussed in detail in Sect. III. Constraints from LFV, particularly the stringent experimental limit on the branching ratio of $\mu \to e\gamma$, exclude a significant portion of the parameter space. The impact of LFV constraints is also visible in the subfigure where χ is the NLOP, even though χ itself does not directly participate in LFV processes. This occurs because the same Yukawa couplings that govern LFV amplitudes

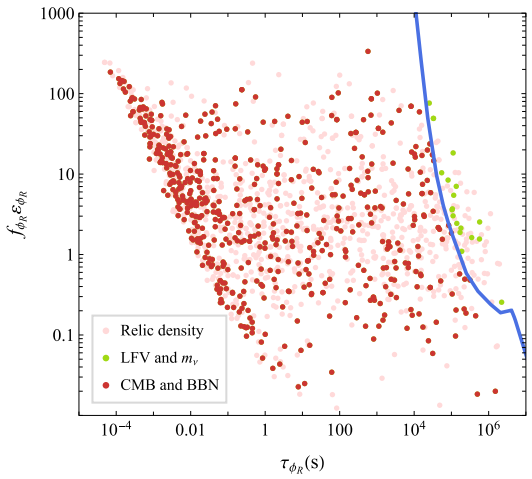

Fig. 8. (color online) Scan results in the $f_{\phi_R}\varepsilon_{\phi_R}$–$\tau_{\phi_R}$ plane for the case in which ϕ_R is the NLOP. The blue curve shows the combined constraints from BBN and CMB as derived in Ref. [80].

also influence the DM production rate, and thus, must satisfy both the relic density and flavor constraints simultaneously. The bounds from BBN and CMB have been discussed previously and are applied depending on the iden-

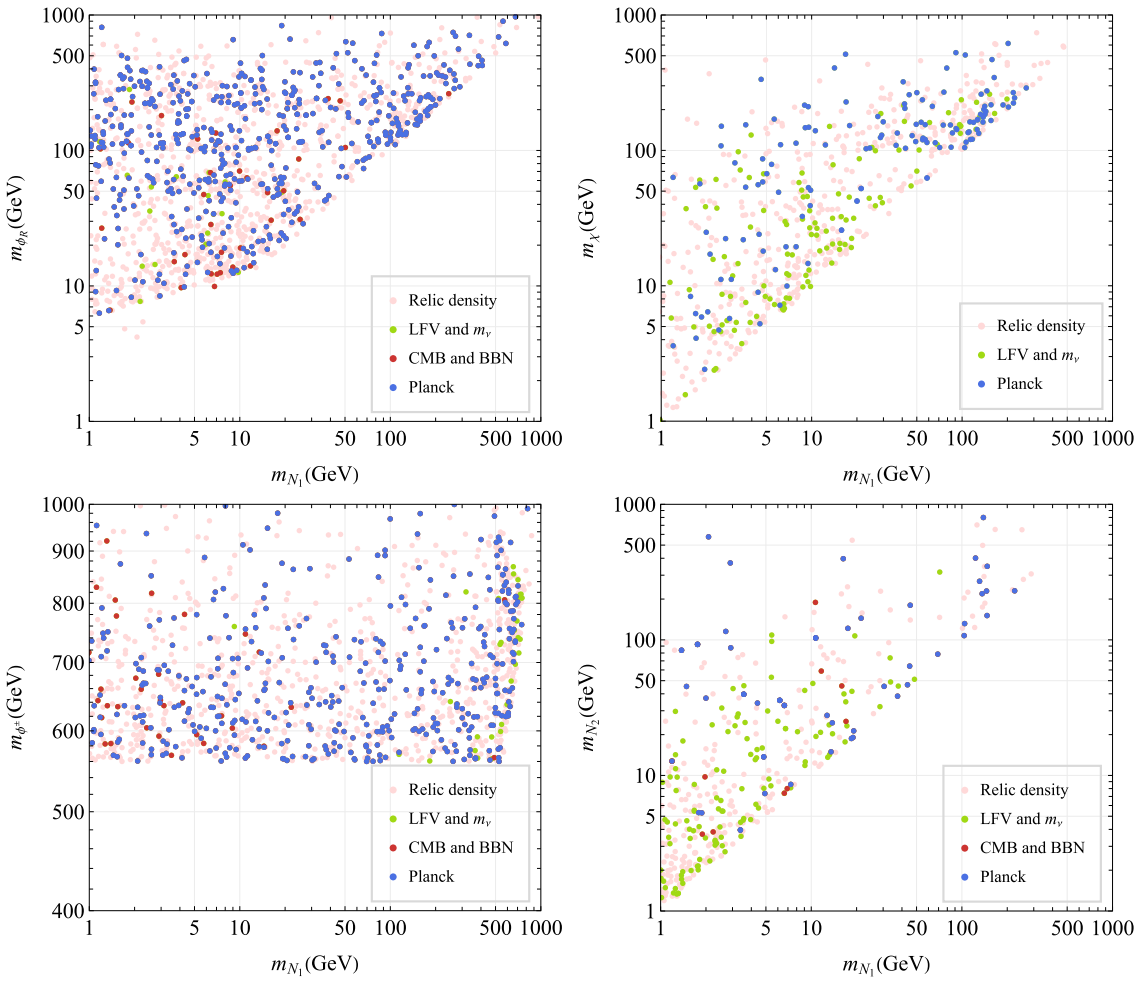

Fig. 9. (color online) Results of the parameter scan in the $m_{\rm NLOP}-m_{N_1}$ plane under combined constraints from the DM relic density, LFV, neutrino mass, CMB, BBN, and $\Delta N_{\rm eff}$.

tity of the NLOP. In all cases—whether ϕ_R, χ, $\phi^\pm$, or N_2 serves as the NLOP—we identify regions of the parameter space that satisfy all observational constraints, including the latest limits on $\Delta N_{\rm eff}$. This demonstrates the viability of the FIMP Scotogenic Dirac Model as a unified framework for explaining both neutrino mass generation and the observed DM relic abundance. Future experiments will play a crucial role in testing this scenario. Long-lived particle searches at facilities such as MATHUSLA [73] could probe the metastable NLOP states, while next-generation CMB observations from CMB-S4 [78] will improve the sensitivity to $\Delta N_{\rm eff}$ and energy injection during cosmic evolution. These experiments will either confirm the model predictions or further constrain its surviving parameter space.

V. CONCLUSION

In this work, we have studied the FIMP Scotogenic Dirac Model, a well-motivated extension of the SM that simultaneously addresses the origin of neutrino masses and nature of DM. The lightest neutral fermion N_1 is a FIMP DM candidate, produced out of equilibrium. Neutrino masses are generated radiatively at one loop, resulting in a rank-2 mass matrix owing to highly suppressed couplings to N_1, thereby predicting one almost massless neutrino. Stringent LFV constraints require the Yukawa couplings $(y_\Phi)_{\alpha 2,3}$ to be small, which in turn necessitates larger $(y_\chi)_{\alpha 2,3}$ to fit the neutrino mass scale. This coupling structure crucially impacts the phenomenology governing the freeze-out dynamics of the NLOP and the thermal history of the right-handed neutrino bath.

We systematically analyzed two distinct production mechanisms for N_1: direct freeze-in via decays of heavier Z_2-odd scalars and fermions, and the "super-WIMP" mechanism, in which N_1 is produced from the late decay of a thermally frozen-out NLOP. The latter scenario leads to rich phenomenology depending on whether N_2, $\phi_{R,I}$, $\phi^\pm$, or χ serves as the NLOP. We demonstrated that the correct relic abundance can be achieved across various benchmarks, with coannihilation effects and enhanced annihilation channels playing crucial roles in regulating the

NLOP's freeze-out density, thereby offering flexible pathways to match the observed DM density.

Another central focus of this work was the cosmological impact on the effective number of relativistic species. Our analysis revealed two distinct contributions to this quantity. The first is a thermal contribution arising from the primordial right-handed neutrino bath. This component is determined by the decoupling temperature of the ν_R bath, which is set by the strength of the interactions between the dark sector and SM plasma. The second contribution is non-thermal, originating from the late decays of the NLOP. The magnitude of this non-thermal contribution is highly sensitive to the NLOP's properties: both a longer lifetime $\tau_{\rm NLOP}$ and larger energy fraction $f_{\rm NLOP}$ lead to a more pronounced heating effect, and thus, a higher $\Delta N_{\rm eff}$.

We performed a comprehensive parameter scan, sequentially applying constraints from the DM relic density, neutrino mass and LFV, BBN/CMB, and $\Delta N_{\rm eff}$. A viable parameter space exists for all NLOP candidates that satisfy all current observational bounds. Future experiments on long-lived particle searches and precision $\Delta N_{\rm eff}$ measurements will provide powerful probes to either discover this framework or constrain its remaining parameter space further.

Finally, it is instructive to contrast the two possible DM production mechanisms in our work: thermal freeze-out (WIMP) [63] versus freeze-in (FIMP). The distinction is most pronounced in the size of the Yukawa couplings $(y_{\Phi,\chi})_{\alpha 1}$ that govern the interaction of the lightest odd particle N_1 with the SM sector. In the WIMP scenario, these couplings must be relatively large to ensure efficient annihilation and avoid overproduction of DM. In contrast, in the FIMP regime, the couplings are extremely suppressed, $(y_{\Phi,\chi})_{\alpha 1} \lesssim 10^{-7}$, keeping N_1 out of thermal equilibrium throughout cosmic history. The relic density is then generated via the slow decay of heavier states, and this suppression naturally leads to a rank-2 neutrino mass matrix, thereby predicting one almost massless neutrino—a feature that is not generic in WIMP realizations. Phenomenologically, the two scenarios are also sharply distinguished by experimental constraints. The WIMP parameter space is heavily constrained: collider searches exclude light DM masses, while direct and indirect detection experiments probe the TeV-scale region. In contrast, FIMPs evade these conventional probes owing to their feeble couplings. Their collider signatures are limited to displaced decays of the NLOP (e.g., displaced vertices), and current long-lived particle searches provide only weak limits. Direct and indirect DM detection signals are negligible. Instead, the primary observational window for FIMPs lies in cosmology — particularly through their contribution to $\Delta N_{\rm eff}$ from late decays of long-lived particles —which offers a powerful and complementary test of the freeze-in paradigm.

ACKNOWLEDGMENTS

We thank Zhi-Long Han, Ang Liu, and Xiao-Dong Ma for helpful discussions.

References

[1] R. Davis, J r., D. S. Harmer, and K. C. Hoffman, Phys. Rev. Lett. **20**, 1205 (1968)

[2] Y. Fukuda *et al.* (Super-Kamiokande Collaboration), Phys. Rev. Lett. **81**, 1562 (1998), arXiv: hep-ex/9807003

[3] F. P. An *et al.* (Daya Bay Collaboration), Phys. Rev. Lett. **108**, 171803 (2012), arXiv: 1203.1669

[4] J. K. Ahn *et al.* (RENO Collaboration), Phys. Rev. Lett. **108**, 191802 (2012), arXiv: 1204.0626

[5] E. Aliu *et al.* (K2K Collaboration), Phys. Rev. Lett. **94**, 081802 (2005), arXiv: hep-ex/0411038

[6] Y. Abe *et al.* (Double Chooz Collaboration), Phys. Rev. Lett. **108**, 131801 (2012), arXiv: 1112.6353

[7] Y. Cai, T. Han, T. Li *et al.*, Front. in Phys. **6**, 40 (2018), arXiv: 1711.02180

[8] A. M. Sirunyan *et al.* (CMS Collaboration), JHEP **01**, 122 (2019), arXiv: 1806.10905

[9] M. J. Dolinski, A. W. P. Poon, and W. Rodejohann, Ann. Rev. Nucl. Part. Sci. **69**, 219 (2019), arXiv: 1902.04097

[10] G. Anton *et al.* (EXO-200 Collaboration), Phys. Rev. Lett. **123**, 161802 (2019), arXiv: 1906.02723

[11] N. Abgrall *et al.* (LEGEND Collaboration), arXiv: 2107.11462

[12] S. I. Alvis *et al.* (Majorana Collaboration), Phys. Rev. C **100**, 025501 (2019), arXiv: 1902.02299

[13] E. Armengaud *et al.* (CUPID Collaboration), Phys. Rev. Lett. **126**, 181802 (2021), arXiv: 2011.13243

[14] S. Abe *et al.* (KamLAND-Zen Collaboration), Phys. Rev. Lett. **130**, 051801 (2023), arXiv: 2203.02139

[15] C. Y. Yao and G. J. Ding, Phys. Rev. D **97**, 095042 (2018), arXiv: 1802.05231

[16] S. C. Chuliá, R. Srivastava, and J. W. F. Valle, Phys. Rev. D **98**, 035009 (2018), arXiv: 1804.03181

[17] J. Calle, D. Restrepo, C. E. Yaguna *et al.*, Phys. Rev. D **99**, 075008 (2019), arXiv: 1812.05523

[18] S. Jana, P. K. Vishnu, and S. Saad, JCAP **04**, 018 (2020), arXiv: 1910.09537

[19] S. Saad, Nucl. Phys. B **943**, 114636 (2019), arXiv: 1902.07259

[20] Y. Farzan and E. Ma, Phys. Rev. D **86**, 033007 (2012), arXiv: 1204.4890

[21] P. H. Gu and H. J. He, JCAP **12**, 010 (2006), arXiv: hep-ph/0610275

[22] P. H. Gu and U. Sarkar, Phys. Rev. D **77**, 105031 (2008), arXiv: 0712.2933

[23] S. C. Chuliá, E. Ma, R. Srivastava *et al.*, Phys. Lett. B **767**, 209 (2017), arXiv: 1606.04543

[24] C. Bonilla, E. Ma, E. Peinado *et al.*, Phys. Lett. B **762**, 214 (2016), arXiv: 1607.03931

[25] W. Wang and Z. L. Han, JHEP **04**, 166 (2017), arXiv: 1611.03240

[26] D. Borah and A. Dasgupta, JCAP **06**, 003 (2017), arXiv: 1702.02877
[27] W. Wang, R. Wang, Z. L. Han *et al*., Eur. Phys. J. C **77**, 889 (2017), arXiv: 1705.00414
[28] S. C. Chuliá, R. Srivastava, and J. W. F. Valle, Phys. Lett. B **773**, 26 (2017), arXiv: 1706.00210
[29] E. Ma and U. Sarkar, Phys. Lett. B **776**, 54 (2018), arXiv: 1707.07698
[30] C. Y. Yao and G. J. Ding, Phys. Rev. D **96**, 095004 (2017), arXiv: 1707.09786
[31] C. Bonilla, J. M. Lamprea, E. Peinado *et al*., Phys. Lett. B **779**, 257 (2018), arXiv: 1710.06498
[32] A. Ibarra, A. Kushwaha, and S. K. Vempati, Phys. Lett. B **780**, 86 (2018), arXiv: 1711.02070
[33] D. Borah and B. Karmakar, Phys. Lett. B **780**, 461 (2018), arXiv: 1712.06407
[34] A. Das, T. Nomura, H. Okada *et al*., Phys. Rev. D **96**, 075001 (2017), arXiv: 1704.02078
[35] S. C. Chuliá, R. Srivastava, and J. W. F. Valle, Phys. Lett. B **781**, 122 (2018), arXiv: 1802.05722
[36] Z. L. Han and W. Wang, Eur. Phys. J. C **78**, 839 (2018), arXiv: 1805.02025
[37] D. Borah, B. Karmakar, and D. Nanda, JCAP **07**, 039 (2018), arXiv: 1805.11115
[38] D. Borah and B. Karmakar, Phys. Lett. B **789**, 59 (2019), arXiv: 1806.10685
[39] C. D. R. Carvajal and Ó. Zapata, Phys. Rev. D **99**, 075009 (2019), arXiv: 1812.06364
[40] E. Ma, Phys. Lett. B **793**, 411 (2019), arXiv: 1901.09091
[41] A. Dasgupta, S. K. Kang, and O. Popov, Phys. Rev. D **100**, 075030 (2019), arXiv: 1903.12558
[42] K. Enomoto, S. Kanemura, K. Sakurai *et al*., Phys. Rev. D **100**, 015044 (2019), arXiv: 1904.07039
[43] S. Jana, P. K. Vishnu, and S. Saad, Eur. Phys. J. C **79**, 916 (2019), arXiv: 1904.07407
[44] E. Ma, Eur. Phys. J. C **79**, 903 (2019), arXiv: 1905.01535
[45] E. Ma, Nucl. Phys. B **946**, 114725 (2019), arXiv: 1907.04665
[46] D. Restrepo, A. Rivera, and W. Tangarife, Phys. Rev. D **100**, 035029 (2019), arXiv: 1906.09685
[47] S. C. Chuliá, R. Cepedello, E. Peinado *et al*., JHEP **10**, 093 (2019), arXiv: 1907.08630
[48] J. Calle, D. Restrepo, and Ó. Zapata, Phys. Rev. D **101**, 035004 (2020), arXiv: 1909.09574
[49] R. Kumar, N. Nath, R. Srivastava *et al*. (2025), arXiv: 2505.01407
[50] Z. A. Borboruah, D. Borah, L. Malhotra *et al*., Phys. Rev. D **112**, 015022 (2025), arXiv: 2412.12267
[51] B. De, D. Das, M. Mitra, and N. Sahoo, JHEP **08**, 202 (2022), arXiv: 2106.00979
[52] X. Luo, W. Rodejohann, and X. J. Xu, JCAP **06**, 058 (2020), arXiv: 2005.01629
[53] X. Luo, W. Rodejohann, and X. J. Xu, JCAP **03**, 082 (2021), arXiv: 2011.13059
[54] S. C. Chuliá, R. Srivastava, and S. Yadav, JHEP **04**, 038 (2025), arXiv: 2409.18513
[55] G. Arcadi, M. Dutra, P. Ghosh *et al*., Eur. Phys. J. C **78**, 203 (2018), arXiv: 1703.07364
[56] Z. Bo *et al*. (PandaX Collaboration), Phys. Rev. Lett. **134**, 011805 (2025), arXiv: 2408.00664
[57] J. Aalbers *et al*. (LZ Collaboration), Phys. Rev. Lett. **135**, 011802 (2025), arXiv: 2410.17036
[58] L. J. Hall, K. Jedamzik, J. March-Russell *et al*., JHEP **03**, 080 (2010), arXiv: 0911.1120
[59] X. Liu, S. Y. Guo, B. Zhu *et al*., Sci. Bull. **67**, 1437 (2022), arXiv: 2204.04834
[60] L. Bian and X. Liu, Phys. Rev. D **99**, 055003 (2019), arXiv: 1811.03279
[61] A. G. Hessler, A. Ibarra, E. Molinaro *et al*., JHEP **01**, 100 (2017), arXiv: 1611.09540
[62] E. Molinaro, C. E. Yaguna, and O. Zapata, JCAP **07**, 015 (2014), arXiv: 1405.1259
[63] S. Y. Guo and Z. L. Han, JHEP **12**, 062 (2020), arXiv: 2005.08287
[64] K. Afanaciev *et al*. (MEG II Collaboration), (2025), arXiv: 2504.15711
[65] A. Alloul, N. D. Christensen, C. Degrande *et al*., Comput. Phys. Commun. **185**, 2250 (2014), arXiv: 1310.1921
[66] G. Alguero, G. Belanger, F. Boudjema *et al*., Comput. Phys. Commun. **299**, 109133 (2024), arXiv: 2312.14894
[67] J. L. Feng, A. Rajaraman, and F. Takayama, Phys. Rev. Lett. **91**, 011302 (2003), arXiv: hep-ph/0302215
[68] R. Barbieri, L. J. Hall, and V. S. Rychkov, Phys. Rev. D **74**, 015007 (2006), arXiv: hep-ph/0603188
[69] L. L. Honorez, E. Nezri, J. F. Oliver *et al*., JCAP **02**, 028 (2007), arXiv: hep-ph/0612275
[70] M. Cirelli, N. Fornengo, and A. Strumia, Nucl. Phys. B **753**, 178 (2006), arXiv: hep-ph/0512090
[71] T. Hambye, F. S. Ling, L. L. Honorez *et al*., JHEP **07**, 090 (2009), arXiv: 0903.4010
[72] G. Aad *et al*. (ATLAS Collaboration), JHEP **07**, 140 (2025), arXiv: 2502.06694
[73] D. Curtin *et al*., Rept. Prog. Phys. **82**, 116201 (2019), arXiv: 1806.07396
[74] G. Mangano, G. Miele, S. Pastor *et al*., Nucl. Phys. B **729**, 221 (2005), arXiv: hep-ph/0506164
[75] E. Grohs, G. M. Fuller, C. T. Kishimoto *et al*., Phys. Rev. D **93**, 083522 (2016), arXiv: 1512.02205
[76] P. F. de Salas and S. Pastor, JCAP **07**, 051 (2016), arXiv: 1606.06986
[77] N. Aghanim *et al*. (Planck Collaboration), Astron. Astrophys. **641**, A6 (2020) [Erratum: Astron. Astrophys. **652**, C4 (2021)], arXiv: 1807.06209
[78] K. N. Abazajian *et al*. (CMB-S4), (2016), arXiv: 1610.02743
[79] V. Poulin, J. Lesgourgues, and P. D. Serpico, JCAP **03**, 043 (2017), arXiv: 1610.10051
[80] T. Hambye, M. Hufnagel, and M. Lucca, JCAP **05**, 033 (2022), arXiv: 2112.09137
[81] M. Lucca, N. Schöneberg, D. C. Hooper *et al*., JCAP **02**, 026 (2020), arXiv: 1910.04619
[82] M. Kawasaki, K. Kohri, and T. Moroi, Phys. Rev. D **71**, 083502 (2005), arXiv: astro-ph/0408426
[83] K. Jedamzik, JCAP **03**, 008 (2008), arXiv: 0710.5153
[84] M. Escudero, JCAP **02**, 007 (2019), arXiv: 1812.05605
[85] M. E. Abenza, JCAP **05**, 048 (2020), arXiv: 2001.04466